

We are IntechOpen, the world's leading publisher of Open Access books Built by scientists, for scientists

4,800

Open access books available

122,000

International authors and editors

135M

Downloads

Our authors are among the

154

Countries delivered to

TOP 1%

most cited scientists

12.2%

Contributors from top 500 universities



WEB OF SCIENCE™

Selection of our books indexed in the Book Citation Index
in Web of Science™ Core Collection (BKCI)

Interested in publishing with us?
Contact book.department@intechopen.com

Numbers displayed above are based on latest data collected.
For more information visit www.intechopen.com



Repair Inspection Technique Based on Elastic-Wave Tomography Applied for Deteriorated Concrete Structures

*Katsufumi Hashimoto, Tomoki Shiotani, Takahiro Nishida
and Nobuhiro Okude*

Abstract

Applying elastic wave tomography as an innovative NDT method, the evaluation of velocity distribution in three-dimensional (3D) before and after the repair is introduced in this study. The increase in the velocity with penetration of the repair material according to the repair effect is identified visually and quantitatively. The 3D tomography technique is newly proposed for one-side access inspection, using drill hammering to generate an elastic wave. Accordingly, the elastic wave velocity distribution result enables to visualize the internal quality of concrete after patch repair is successfully done. In addition, an attempt for reinforced concrete (RC) slab panels is made to confirm the effectiveness of the repair by comparing the velocity distribution of elastic waves obtained from acoustic emission (AE) tomography analysis, before and after the repair. Thus, the velocity recoveries due to injection are found in all the slab panels, and it is confirmed that the elastic wave velocities obtained using this technique can serve as an indicator for examining the state of crack and void filling with injected material. Further, a good correlation is found between the low-velocity region before repair and the amount of injection. These results show the potential of the AE tomography technique to be used as a method for estimating the effect of injection repair.

Keywords: elastic wave, acoustic emission, wave velocity distribution, tomography, repair method

1. Introduction

It is highly demanded to establish sufficient management systems for the inspection of existing concrete infrastructures in order to manage and extend their service lives. As for aging infrastructure, severe deterioration is currently reported, where it is known as a critical issue in our society, and large budgets are required to repair damaged structures. Since budgetary restrictions are often imposed, preventive and proactive maintenance techniques of infrastructure are sufficiently needed with nondestructive testing (NDT) methods. In addition to conventional NDT, innovative methods must be established to appropriately assess and evaluate

damage and repair and retrofit recovery in concrete structures. Inspection techniques after crack repair methods application for existing structures to assess repair installations have not yet been practically developed, meanwhile improper repair efforts have resulted in re-deterioration. Refilling internal cracks with repair materials from the concrete surface, epoxy injection, and patch repair methods are widely implemented. In most cases, re-deterioration could be led by the unknown and remained internal defects. Consequently, it is very important to implement and establish inspection techniques which can visualize internal defects as a counter-measure with repair works.

For such infrastructure as bridges and tunnels, it is generally recognized that appropriate maintenance works are necessary. Prior to extensive damage and failure in existing structures, essential issues include establishing a maintenance system for reinforced concrete (RC) members with the sufficient measures. Epoxy injection and patch repair methods have been widely and practically introduced to repair and re-strengthen RC members. However, insufficient repair works are unfortunately often reported, and these works have potentially resulted in re-deterioration because more improvement is needed for inspection techniques to estimate the quality of repair and recovery.

Developing nondestructive testing and evaluation methods is strongly demanded for concrete structures to quantify or assure the repair and retrofit recovery. The International Union of Laboratories and Experts in Construction Materials, Systems, and Structures (RILEM) launched a technical committee on innovative NDT for repair and retrofit recovery [1]. Tomography techniques are studied based on elastic wave and acoustic emission (AE) to visualize, internal defects in three-dimension concrete with the committee's activities. These techniques applicability has already been published in terms of elastic wave tomography [2, 3] and AE tomography [4, 5].

Using parameters of elastic wave such as amplitudes and elastic wave velocities, internal distributions are obtained by the tomography technique. Elastic wave velocity is specifically used as the parameter in this study. Both the location of the excitation and the excitation time are known in the mentioned elastic wave tomography. On the other hand, they are unknown for AE tomography. The elastic wave velocity in each set-element over the structure can be calculated. Elastic wave velocity is theoretically associated with elastic modulus of material. The values would vary as low-velocity zones with the presence of such internal defects as cracks and voids.

In a theory of elastic wave propagation inside media, the waves are reflected, diffracted, and scattered where it has voids and cracks. Elastic wave velocity is known to be decreased by the phase divergence. The zones of lower elastic wave velocity corresponding to those of heavier deterioration can be reasonable assumed. The distribution of wave velocities can be accordingly referred to as a good indicator of the internal condition of a concrete structure. Moreover, in order to guarantee whether the injected material is properly filled into cracks by using the crack injection method, the velocity distributions of elastic waves in the applicable regions of RC structures are estimated, before and after the repair, by employing AE tomography method [6].

The repair effects in concrete were evaluated with 3D elastic wave tomography in the present study by means of innovative NDT, which can visually identify the outcome from the repair condition provided by the epoxy injection and patch repair methods. 3D tomography was employed for a 50-year-old concrete pier, which was repaired by epoxy injection method, as well as to a 53-year-old concrete wall, which was repaired by the patch repair method. And, AE tomography was applied to a 46-year-old RC slabs, in which epoxy-based resin was used as the injected material to repair the internal cracks.

As described here, although the epoxy injection and patch repair methods are major repair methods even without the corrosion of the reinforcing bars, there are many reports indicating re-deterioration with insufficient repairs. This study aims to validate the 3D elastic wave tomography and AE tomography technique for inspection of the internal quality of concrete after repair.

2. Examples of existing concrete structures for repair inspection

2.1 Pier

Concrete pier specimen, 600 mm width, 1200 mm height, and 300 mm thickness, is shown in **Figure 1**. About 93 components of syringe-type caulking guns were set into pots for injection and 50 kHz resonance AE sensors were arrayed to receive elastic waves before the injection and 7 days after injection, which is corresponding to the epoxy resin hardening period.

Attached AE sensors to four sides of the pier, as shown in **Figures 2 and 12** sensors were arranged on sides A and B in a 600×1200 mm area and 4 sensors were installed on the other sides. About 25 mm diameter steel ball was used for the excitation of elastic wave. In order to identify the impact excitation time, at the closest sensor location, each excitation point was selected.

2.2 Wall

Figure 3 shows concrete wall, 600×600 mm, where the patch repair method was applied, following V-shaped concrete removal was conducted for 80 mm depth and 120 mm width since surface cracks with water leakage were observed on the



Figure 1.
Overview of concrete pier.

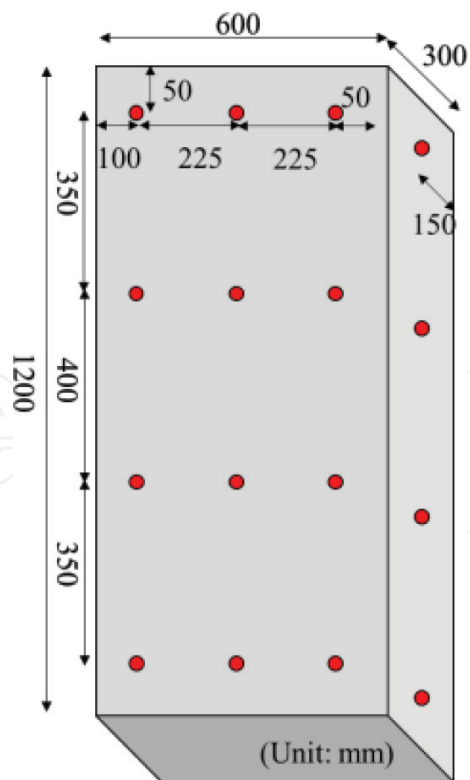


Figure 2.
Sensor arrangement.

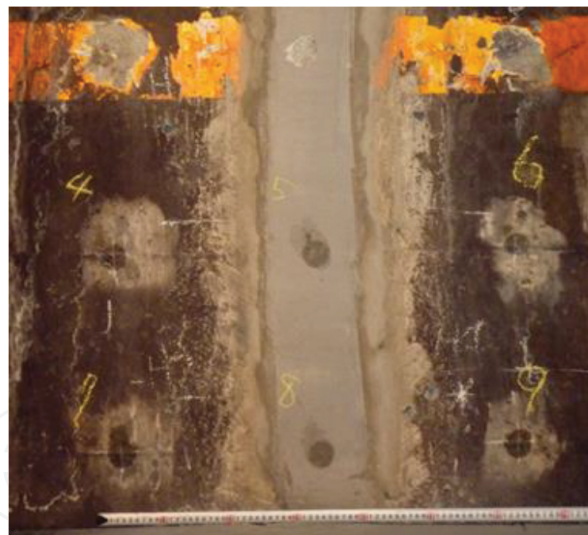


Figure 3.
Overview of concrete wall.

surface of the tunnel-lining concrete. Then, polymer cement mortar with a water-to-cement ratio $W/C = 25\%$ was used to fill the crack. Employing micro-core drilling and hammering as one-sided access measurement, the wave signals generated inside the concrete were detected. A 12 mm diameter micro-coring was performed up to 200 mm depth. A curved edge 6 mm diameter steel bar was inserted into the bit hole. The head of steel bar was hit by 25 mm diameter spherical steel ball. Hammering the steel bar without touching the hole wall, elastic waves could only be generated at the hole end in the depth direction. About 60 kHz resonance AE sensors were installed to detect the elastic waves. The sensor arrangements and excitation points are shown in **Figure 4**.

2.3 Slab

Figure 5 and Table 1 show a top view of an RC bridge, and specifications for the measured deck panels. This bridge is a municipal road bridge located in the Hokuriku region, Japan and it has been in service in the last 46 years. Three panels

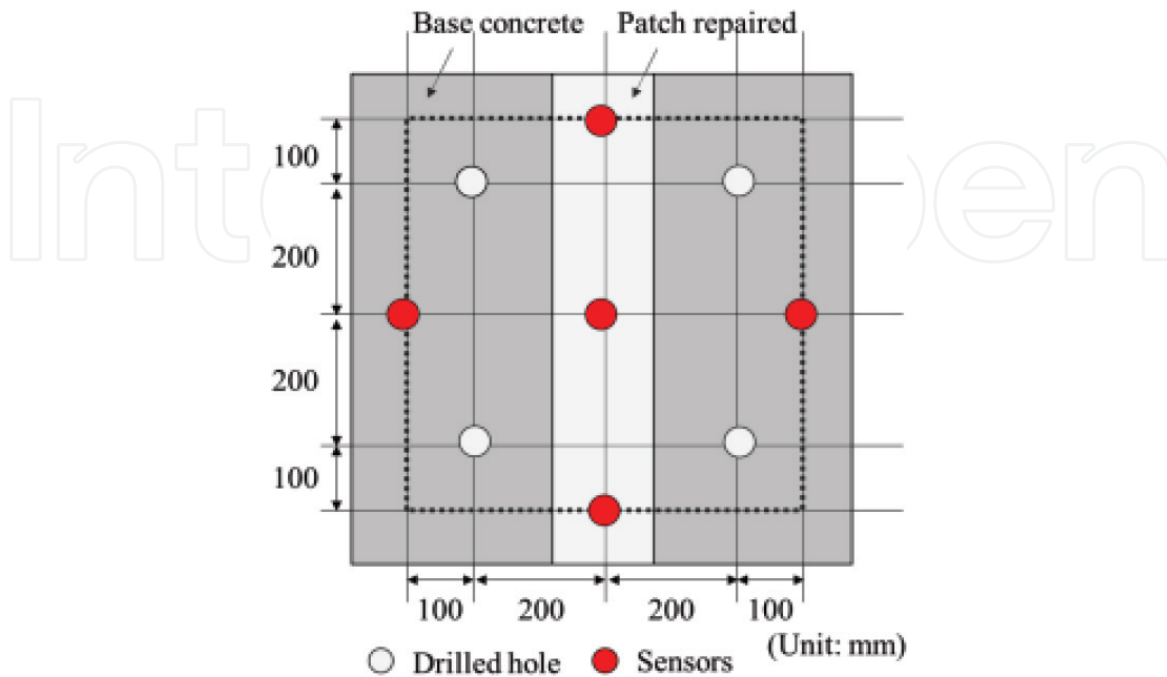


Figure 4. Locations of drilling and sensor arrangement.

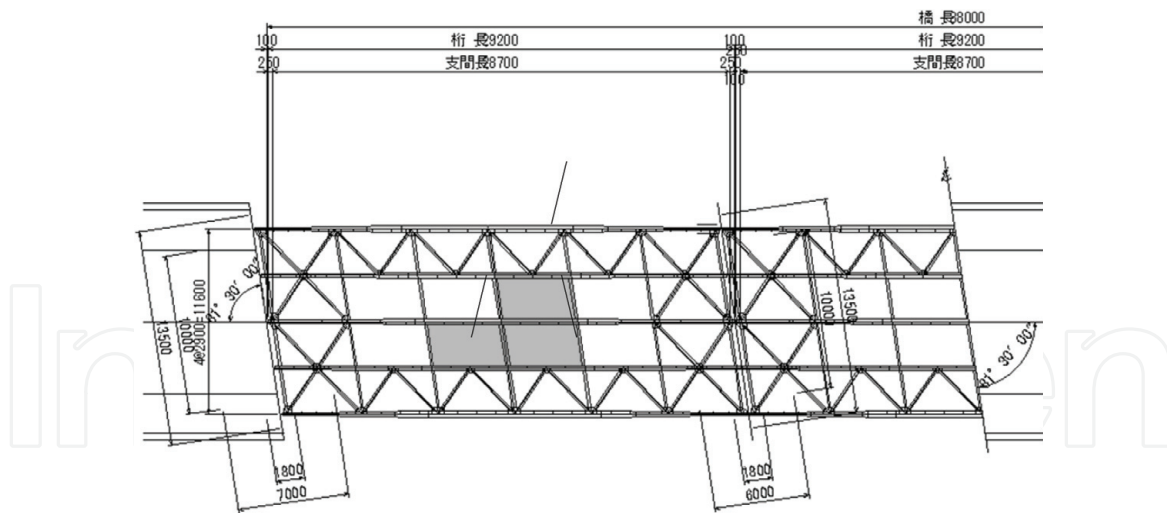


Figure 5. A top side view of subject bridge.

Type	RC bridge (3 span composite girder bridge)
Length	88.0 m
Age	46 years
Thickness	Slab: 250 mm and asphalt: 50 mm
Condition	Web-shaped cracks were sporadically evident on the concrete surface.

Table 1. Bridge specifications.

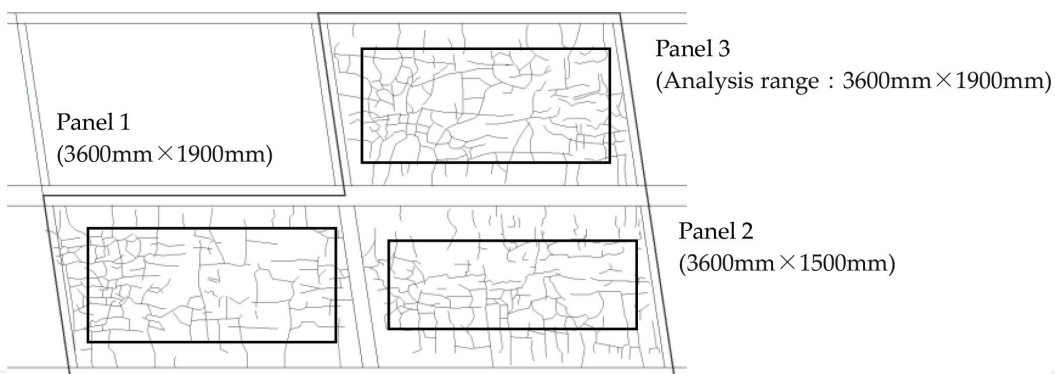


Figure 6.
Sketch of cracking.

highlighted in the figure are selected for the measurement. On all of the slab panels, web-shaped cracks were sporadically evident on the concrete surface. These cracks are thought to be caused primarily by the alkali-silica reaction in concrete. **Figure 6** shows a sketch of cracks obtained through visual inspection from the bottom side of the slab. This figure also shows the area of the tomography analysis for obtaining the velocity distribution. Crack widths are not indicated in figure, but in all the slab panels, the cracks width was smaller than 0.2 mm, and over almost the entire range, the widths were in the range of 0.10–0.15 mm.

3. Data analysis

3.1 Wave detection and computation of elastic wave arrival time

In order to determine the velocity distributions by tomography, the following analytical steps are taken.

First, the arrival time at each sensor was determined with an Akaike Information Criterion (AIC) picker [7, 8]. For the digitized wave record x_k of length N , the AIC value is defined as

$$\begin{aligned} \text{AIC}(k) = & k \times \log \{ \text{var}(x[1, k]) \} \\ & + (N - k - 1) * \log \{ \text{var}(x[k + 1, N]) \} \end{aligned} \quad (1)$$

where $\text{var}(x[1, k])$ indicates the variance between x_1 and x_k , and $\text{var}(x[k, N])$ is the variance between x_k and x_N .

The point where AIC value minimizes, applying the least-square method, corresponds to the most suitable separation point of two series of stationary time, the arrival time as the phase onset is thus reasonably determined by the AIC picker. Lower AIC values suggest noise and higher AIC values show the arrival of wave signals. Following the determination of arrival time, the elastic wave velocity is calculated. The observed time of wave propagation T_{obs} is obtained by [9].

$$T_{obs} = T_o - T_s \quad (2)$$

where T_s is the time of excitation and T_o is the arrival time.

3.2 Elastic wave tomography

The reciprocal of the velocity is referred in the elastic wave tomography algorithm to as the “slowness.” As shown in **Figure 7**, slowness as the initial parameter

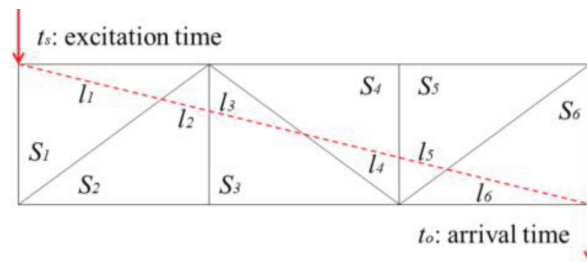


Figure 7.
 Slowness for calculation of propagation time.

is provided into each element. Travel time of elastic wave can be computed as elastic velocity is constant in individual element on this ray path. The total of the propagation time calculated by the slowness and the distance in each element (refer to Eq. (3)) derives the propagation time T_{cal} . The difference between the observed propagation time (T_{obs}) and the theoretical propagation time (T_{cal}) is obtained by Eq. (4).

where l_j is the length crossing each element and s_j is the slowness of each element.

$$T_{cal} = \sum_j s_j * l_j \quad (3)$$

$$\Delta T = T_{obs} - T_{cal} \quad (4)$$

s_i is slowness of element i , l_i is length of the ray path in element i . Thus, it is revealed that l_i is essential for the calculation of the travel time.

In order to reduce the difference between the observed propagation time and the theoretical propagation time, the slowness in each element is re-calculated and renewed. The total slowness correction is determined by Eq. (5) and the revised slowness is consequently calculated by Eq. (6).

$$\begin{bmatrix} \Delta s_1 \\ \Delta s_2 \\ \vdots \\ \Delta s_j \end{bmatrix} = \begin{bmatrix} \frac{\sum_i \frac{\Delta T_i * l_{i1}}{L_i}}{\sum_i l_{i1}} \\ \frac{\sum_i \frac{\Delta T_i * l_{i2}}{L_i}}{\sum_i l_{i2}} \\ \vdots \\ \frac{\sum_i \frac{\Delta T_i * l_{ij}}{L_i}}{\sum_i l_{ij}} \end{bmatrix} \quad (5)$$

$$s'_j = s_j + \Delta s_j \quad (6)$$

where L_i is the total distance of wave propagation through the i -element.

Proceeding the iteration based on Eqs. (5) and (6) as shown in **Figure 8**, the optimal slowness, eventually the velocity, in each element corresponding to the observed propagation times of multiple paths over the interested area is determined as well as the velocity distribution.

In order to determine the ray path more accurately, the ray trace algorithm is applied, taking into account detours of elastic waves due to the reflection and diffraction. Following 3D ray trace algorithm, which was proposed in previous research [3], the arrival time of each wave is obtained. Correction of the slowness in each element is carried out according to the error between the observed first travel time and computed value in the element, using 3D finite elements for meshing of target space in the present algorithm. Wave velocities between 2000 and 4500 m/s are given for the tomography results as the range of wave velocities in concrete.

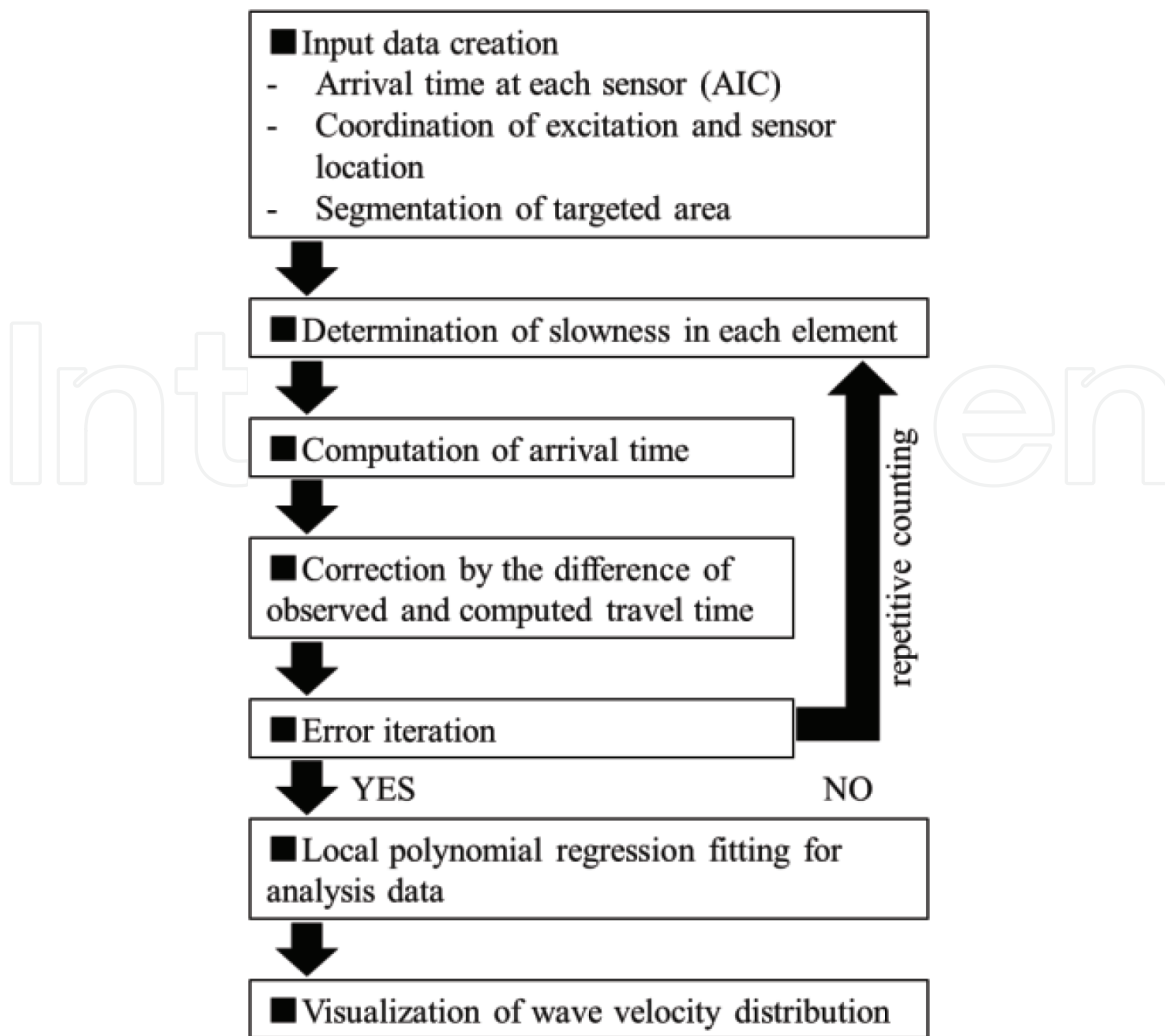


Figure 8.
Analytical procedure for 3D tomography.

3.3 Acoustic emission (AE) tomography

AE tomography is a method for obtaining a velocity distribution by finding the travel time from an AE source to each sensor. Thus, it is necessary to obtain the position of the transmission source as accurately as possible. With the conventional ranging technique, which assumes that the propagation velocity is fixed, considerable errors are expected in the case that the tomography technique is applied to such a heterogeneous material as concrete. Consequently, a new ranging technique incorporating with the ray tracing concept has been developed as a pre-processing technique for AE tomography [6]. The ranging technique using ray tracing is illustrated in **Figure 9**. As shown in the diagram, ray tracing is performed from the received point j to all other nodes i , and the theoretical travel time T_{ji} to each node is calculated. The shortest transmission time is determined from the differences between T_{ji} and the initial travel time T_j at the received point j . The procedure is repeated for the number of received points N , and finally the node, where the variance of estimated arrival times estimated from Eqs. (7) and (8) becomes the minimal, is taken to be the transmission point. In Eq. (7), T_{mi} is the mean value of the estimated transmission times at each node i , and in Eq. (8), σ_i is the variance of the estimated transmission times at each node i .

$$T_{mi} = \frac{\sum_j (T_{ji} - T_j)}{N} \quad (7)$$

$$\sigma_i = \frac{\sum_j (T_{ji} - T_j - T_{mi})^2}{N} \quad (8)$$

3.4 Excitation method of elastic waves and analysis model

Figure 10 shows the model of AE tomography analysis and the positions of receiving sensors. The shaded part at the top of the model indicates the asphalt layer (thickness: 50 mm). Analyzed regions for slab panels 1 and 3 were set to be 3600 × 1900 mm. Concerning slab panel 2, there were limitations on the sensor positions, and thus the region was set to be 3600 × 1500 mm. As elements for AE tomography analysis, the applicable region was divided by 16 × 8 in total of 128 elements. In AE tomography, elastic waves were excited by the steel ball drop. A steel ball of 5 mm diameter was dropped at several locations for 12 minutes from the asphalt surface, consciously ensuring that the distribution of impact points was as uniform as possible at the target area. The steel ball dropping is illustrated in

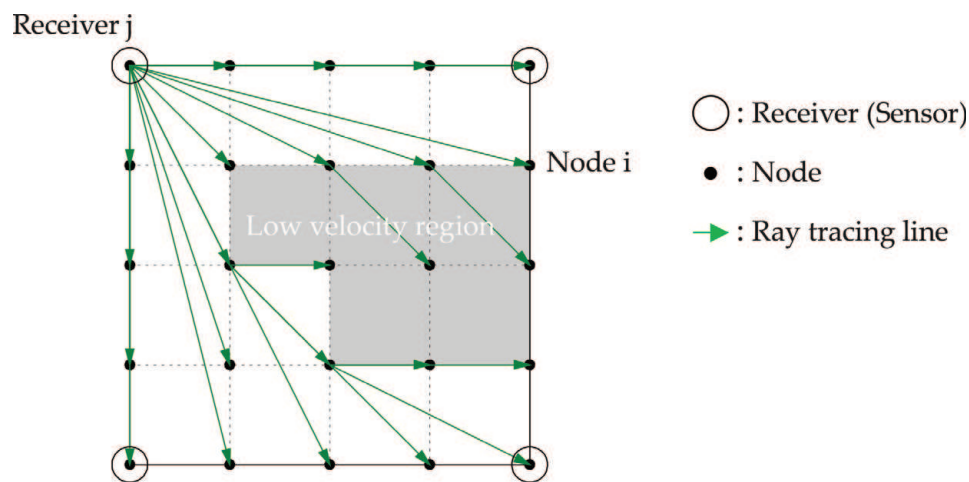


Figure 9.
 Overview of transmission source estimation using ray tracing.

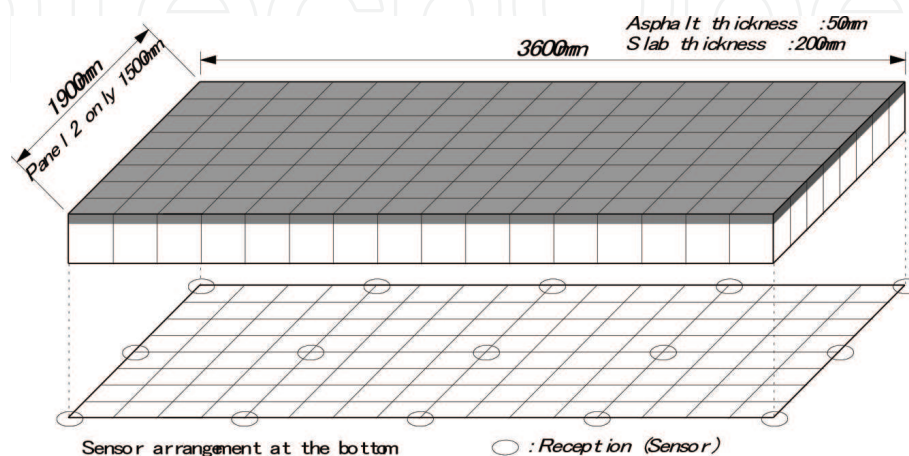


Figure 10.
 Analysis model for AE tomography.



Figure 11.
Steel ball dropping.

Figure 11. In AE tomography, the measurements were performed using an acceleration measurement system (TEAC). About 15 piezoelectric accelerometers with the frequency response from 3 Hz to 15 kHz were employed as receiving sensors. The point at which AIC is the minimum is determined as the arrival time of the wave. However, when the S/N ratio is low, it is difficult to identify the minimum value of AIC. Thus, a reliability parameter is developed for reading the initial travel time. The index is proposed as a measure for the identification of the rising edge of the wave [10]. It is found that readings of the initial travel times reasonably converge if the index is 0.05 or higher. In the present chapter, elastic waves with the index of 0.1 or higher are analyzed. AIC (k_{\min}) indicates the minimum value of AIC, that is, corresponding to the initial travel time.

4. Results and discussion

4.1 Pire

4.1.1 Wave detection and computation of elastic wave arrival time

In order to investigate the epoxy-injected situation in damaged concrete, black light (ultraviolet light) was irradiated on the cored sample so that the injected material (epoxy resin) was colored in blue as shown in **Figure 12**. It is confirmed that epoxy resin was successfully injected into the concrete cover (up to 10 cm) and over the depth of the reinforcing bars (from 10 to 15 cm). The injected material can penetrate cracks even smaller than 0.1 mm in width [11].

4.1.2 3D elastic wave tomography

Figure 12 shows elastic wave tomography results before and after epoxy injection. The overview of injection repair method is shown in **Figure 13**. The wave velocities after the repair indicate clearly higher values than those before. The velocities are mostly higher than approximately 3000 m/s. This result implies that the epoxy injected from the surface of the pier could be filled and hardened sufficiently inside the media via cracks. However, at the central portions of the concrete pier, wave velocities are still lower than 2500 m/s, namely, the epoxy injection only guarantees the shallow zone repair from the concrete surface. The velocity

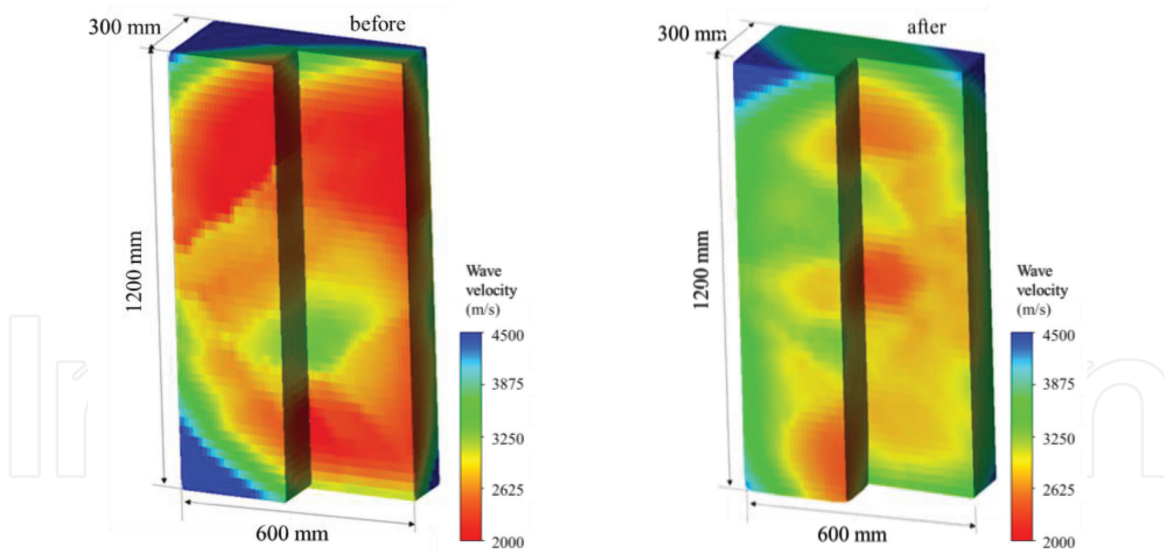


Figure 12.
Results of elastic wave tomography in 3D (left: before injection and right: after injection).



Figure 13.
Repair by epoxy injection.

distribution given by 3D elastic wave tomography shows the conditions inside the concrete, in particular, whether the epoxy is fully penetrated into the interior, while it is noted that the tomography technique could assess the repair level, which is not visually clarified on the exterior.

Figure 14 shows wave velocity histogram before and after the repair consequences. The mean value after the repair is higher than that before, and the variation decreases. Since the velocities lower than 2500 m/s are rarely observed in the histogram, concrete of the pier is repaired after the injection.

4.1.3 Amount of epoxy injection and alteration of wave velocities

Figures 15 and **16** respectively show the tomography results the injected epoxy amount at Side A (referred as the front surface in **Figure 12**) and those at Side B (referred as the back surface in **Figure 12**). They are only the tomograms of wave velocities at the surface layer, comparing with the amount of epoxy injection. The injection pots which added syringe refilling are colored in red because the caulking guns were replaced and refilled with epoxy until the spring-loaded gun automatically stopped the injection.

The velocity distribution alteration reasonably correlates with the epoxy injection amount. Concrete property improvement suggested by the velocity recovery is also roughly confirmed with the epoxy injection amount.

Velocity-improved areas in **Figures 15** and **16** are relatively observed in the areas, where additional injection was installed because of their porous media due to heavy deterioration (red colored in **Figures 15(d)** and **16(d)**). Less improvement of the velocity are observed even after the repair at the bottom-right corner of side A (see **Figure 15**), where the method did not enable to penetrate the resin sufficiently into the concrete because of their lower connectivity of internal cracks.

4.2 Wall

3D elastic wave tomography technique mentioned above was challengingly applied to confirm patch repair effect for concrete wall of an existing structure. In this study, the technique was introduced as a method to evaluate the retrofit recovery. There is currently no NDT technique applicable in terms of in-situ measurement.

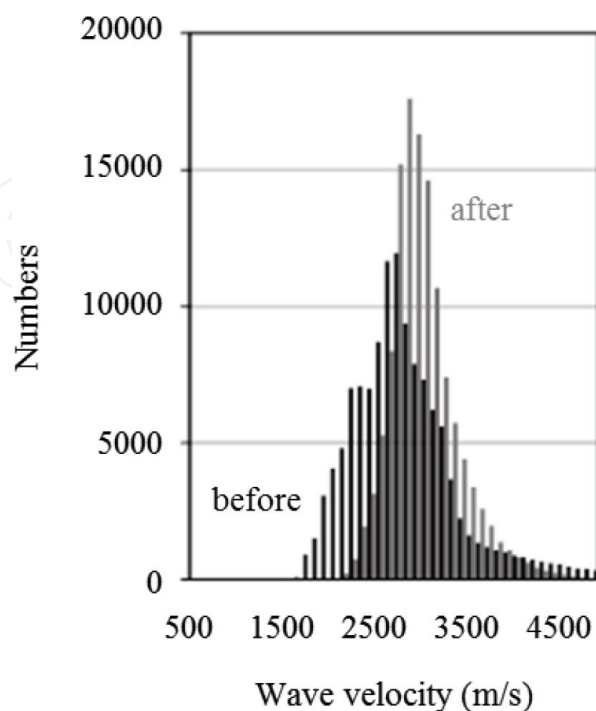


Figure 14.
Histogram of wave velocities.

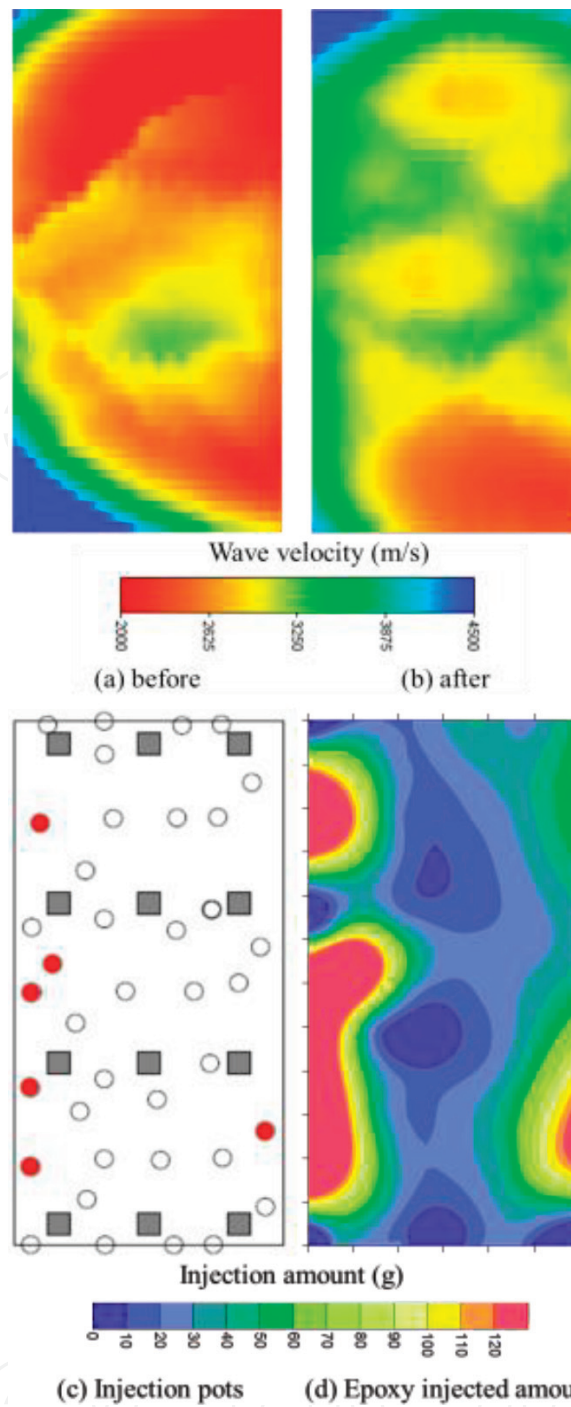


Figure 15.
Results of wave velocities and amount of epoxy injection (Side A).

4.2.1 Procedures of drilling and excitation

Introducing micro-core drilling, excitation of elastic waves was driven. The technique is proposed and applied usefully for one-side access inspection works. **Figure 17** shows the illustration of test procedure schematically.

On the surface of concrete wall with a surface crack (a), a V-cut concrete removal is performed (b), followed by a patch repair method with polymer cement mortar grouting (c), 12 mm diameter bit hole of 200 mm depth is drilled by micro-coring (d), at each concrete surface point. With the sensor array on the surface (e), 6 mm diameter a steel bar is inserted into the hole and the steel bar head is hit by a 25 mm diameter steel sphere ball.

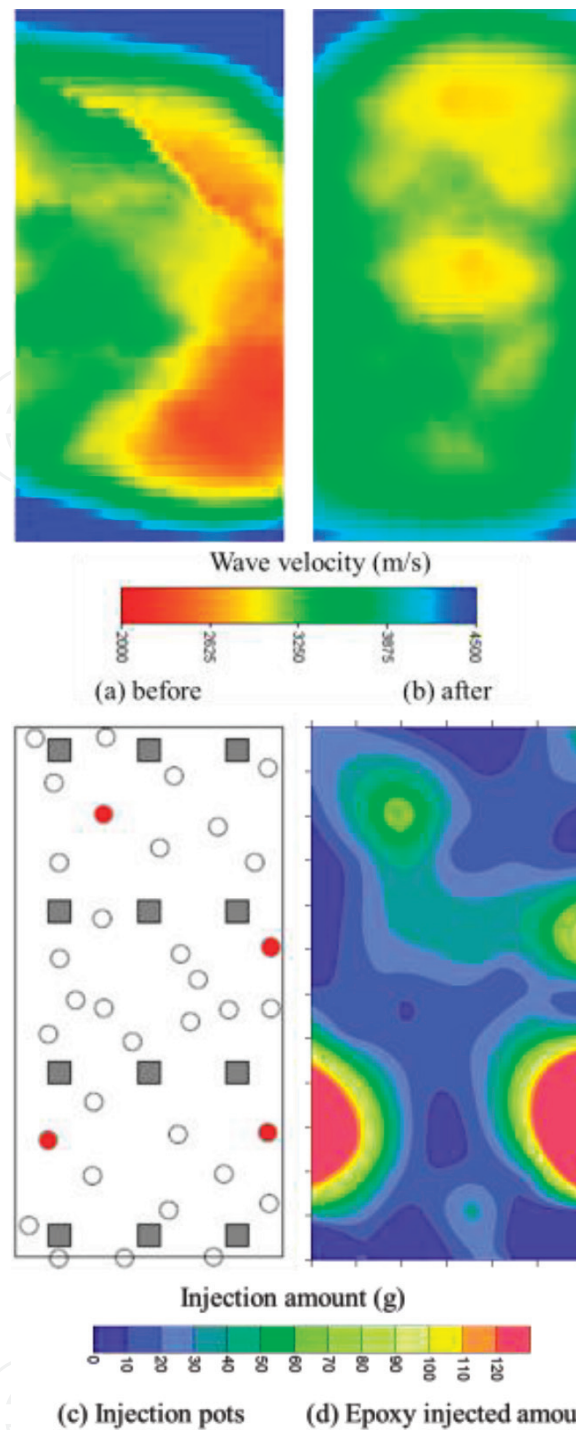


Figure 16. Wave velocity and epoxy injection result (Side B).

Careful hammering at the steel bar head to prevent contacting the hole wall, the excited elastic waves were generated only from the bit hole bottom into the lining concrete, so that the excited signals were detected finally at sensors located on the concrete surface.

4.2.2 Propagation of waves in steel bar

The travel time along the steel bar was measured by two sensors as shown in **Figure 18**. AE sensor A records the excitation time at the head by using a steel ball of 15 mm diameter and the elastic wave travel time in the bar is calculated by

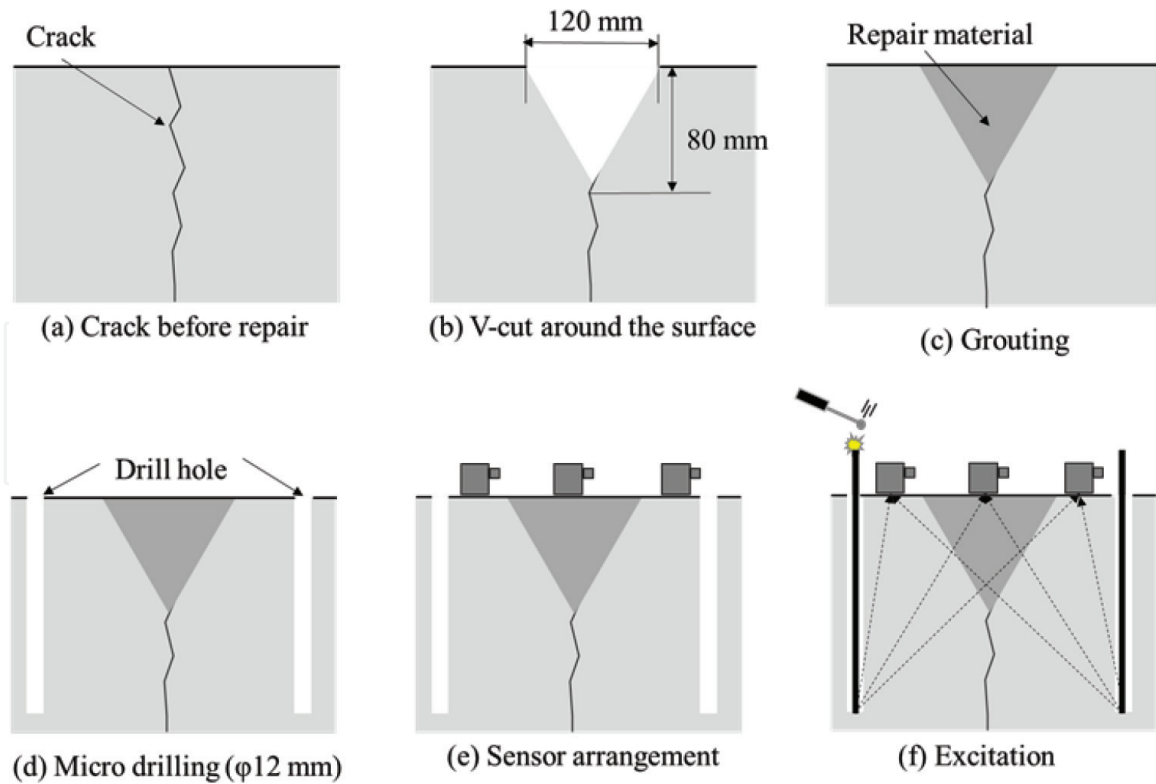


Figure 17.
 Procedures of drilling and excitation.

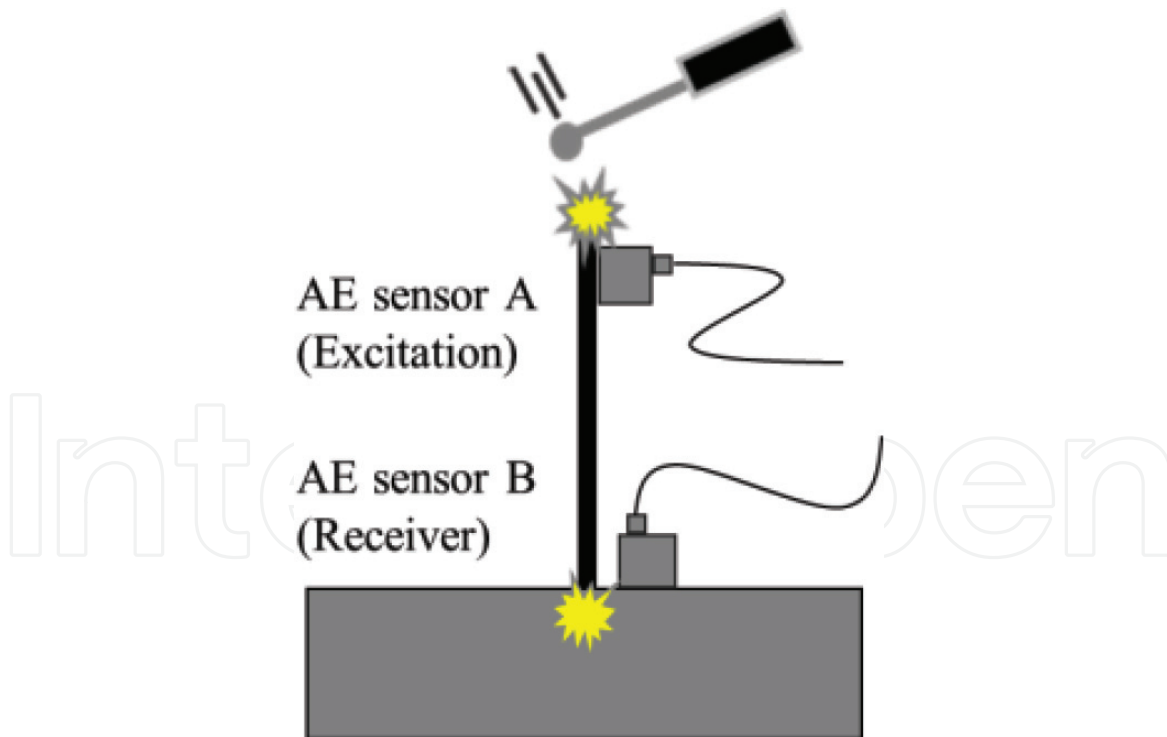


Figure 18.
 Measurement method of travel time in the steel bar.

detecting the arrival time of the wave at AE sensor B. The arrival time difference is $69 \mu\text{s}$ as shown in **Figure 19**.

The dominant frequency of elastic wave excited by a 15 mm diameter steel ball is known as 19.4 kHz according to [12]. Considering a steel bar is used as wave guide, a frequency analysis was conducted for the waveforms observed at A and B.

Figure 20 shows the frequency spectra. Each guided wave is detected via the 38 mm length steel bar. The dominant frequency was observed at A for 22.5 kHz and the dominant frequency was 16.6 kHz at B. Since these detected frequencies are higher than the resonant frequencies of the steel bar, first flexural mode (1.1 kHz), second flexural mode (3.2 kHz), and third flexural mode (5.4 kHz), respectively, as a cantilever, the principal components of the waveform were assumed to be generated as compression wave excited by the tapping at steel bar head.

4.2.3 3D elastic wave tomography

The computation for wave velocity distribution in the targeted concrete wall was implemented by the tomography technique mentioned previously. **Figure 21** shows the 3D distribution of wave velocities and **Figure 22** shows them at cross section A.

Although the triangle-shaped (dashed line) repair area has high velocity on the surface, the V-shaped low-velocity area is observed toward the bottom, whereas high-velocity zones exist at the left side of the specimen. The high velocity may

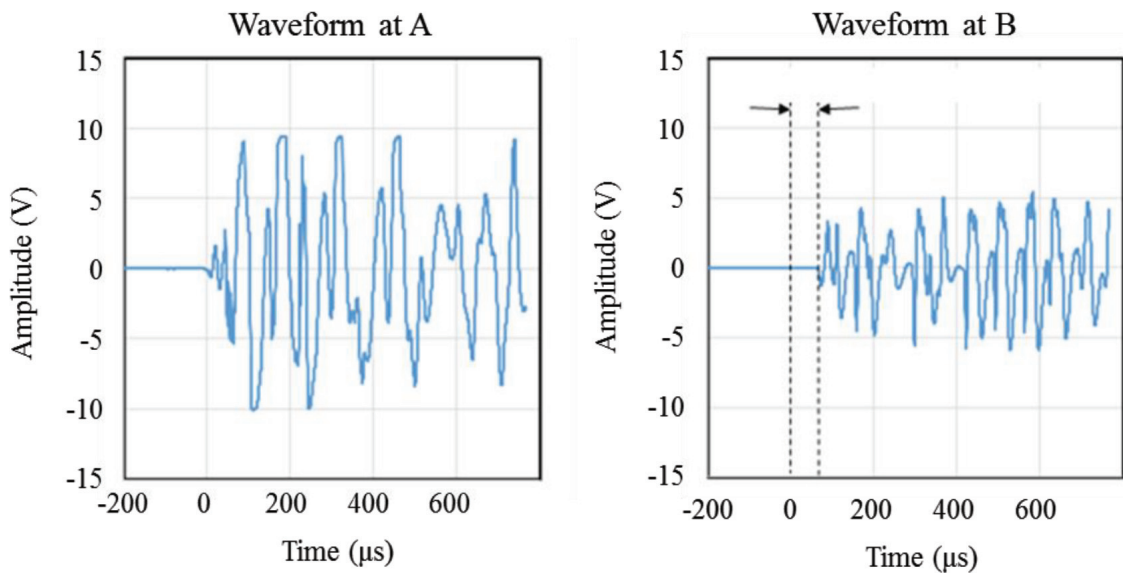


Figure 19.
Waveforms at excitation and receiver.

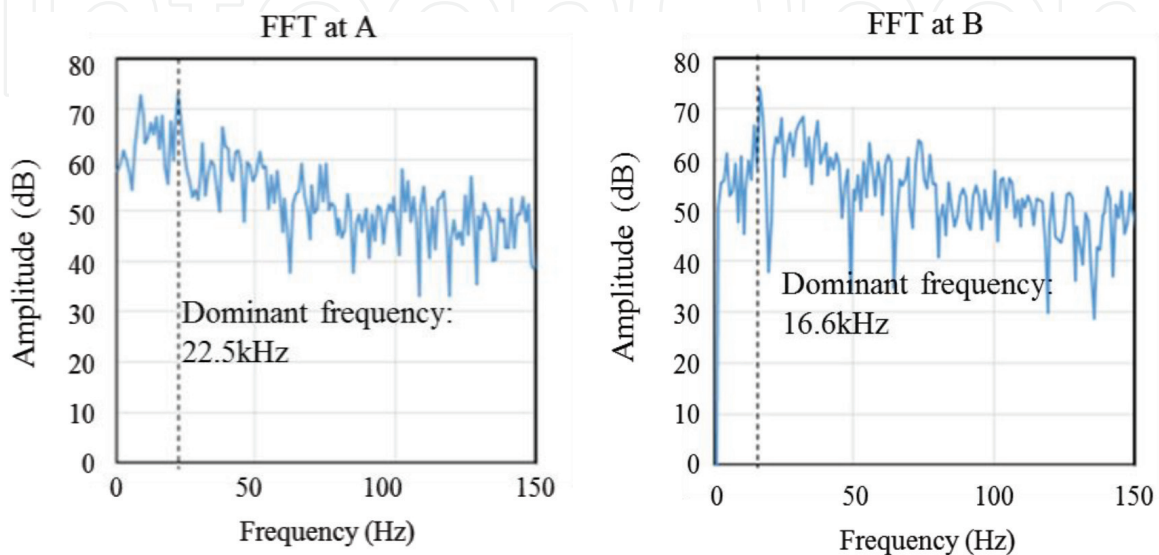


Figure 20.
Frequency spectra of waveforms at A and B.

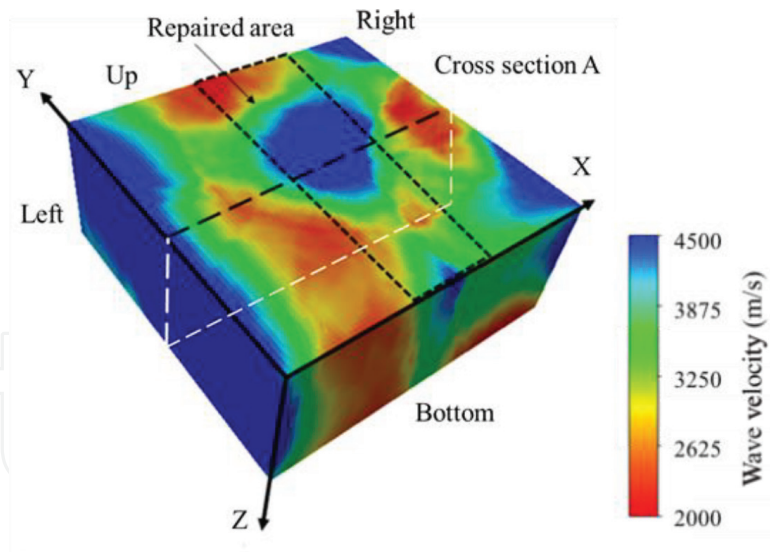


Figure 21.
Distribution of wave velocities in 3D.

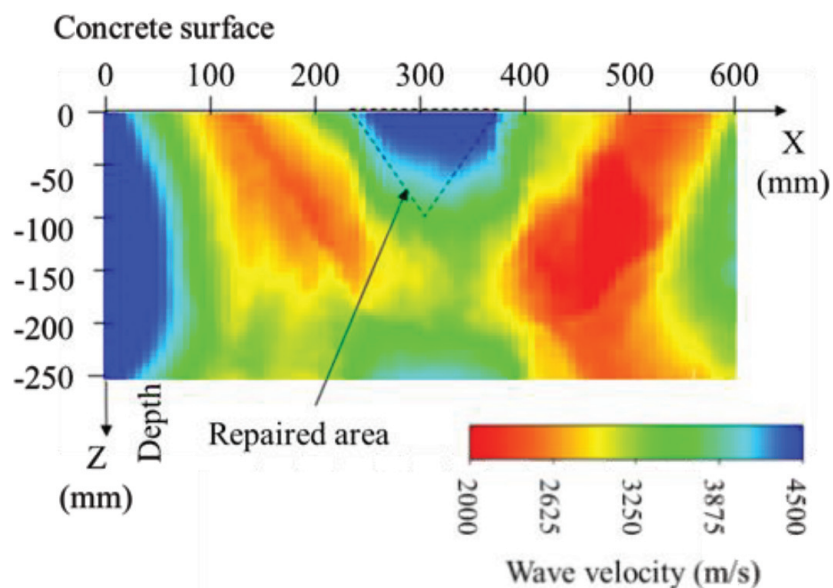


Figure 22.
Distribution of wave velocities at cross section A.

indicate the intact condition of the original concrete quality, because the interested area is enough far from the repaired area.

The repaired part is denoted by high velocity, in **Figure 22**, meanwhile the original concrete surrounding the patched area remarkably shows low velocity. The V-shaped area with low velocity underneath the repaired part could be potentially damaged by the chipping work for concrete removal. This is generally known and described in concrete surface treatment guideline prior to repairs and overlays [13, 14]. Further investigation is needed for the consideration in the influence of the hammer drill impact on damage to the concrete behind the removal zone.

4.3 Slab

4.3.1 Velocity distribution of AE tomography

Figure 23 shows the results of AE tomography, before and after repair by means of the crack injection. Results show that in all the slab panels, the velocity after

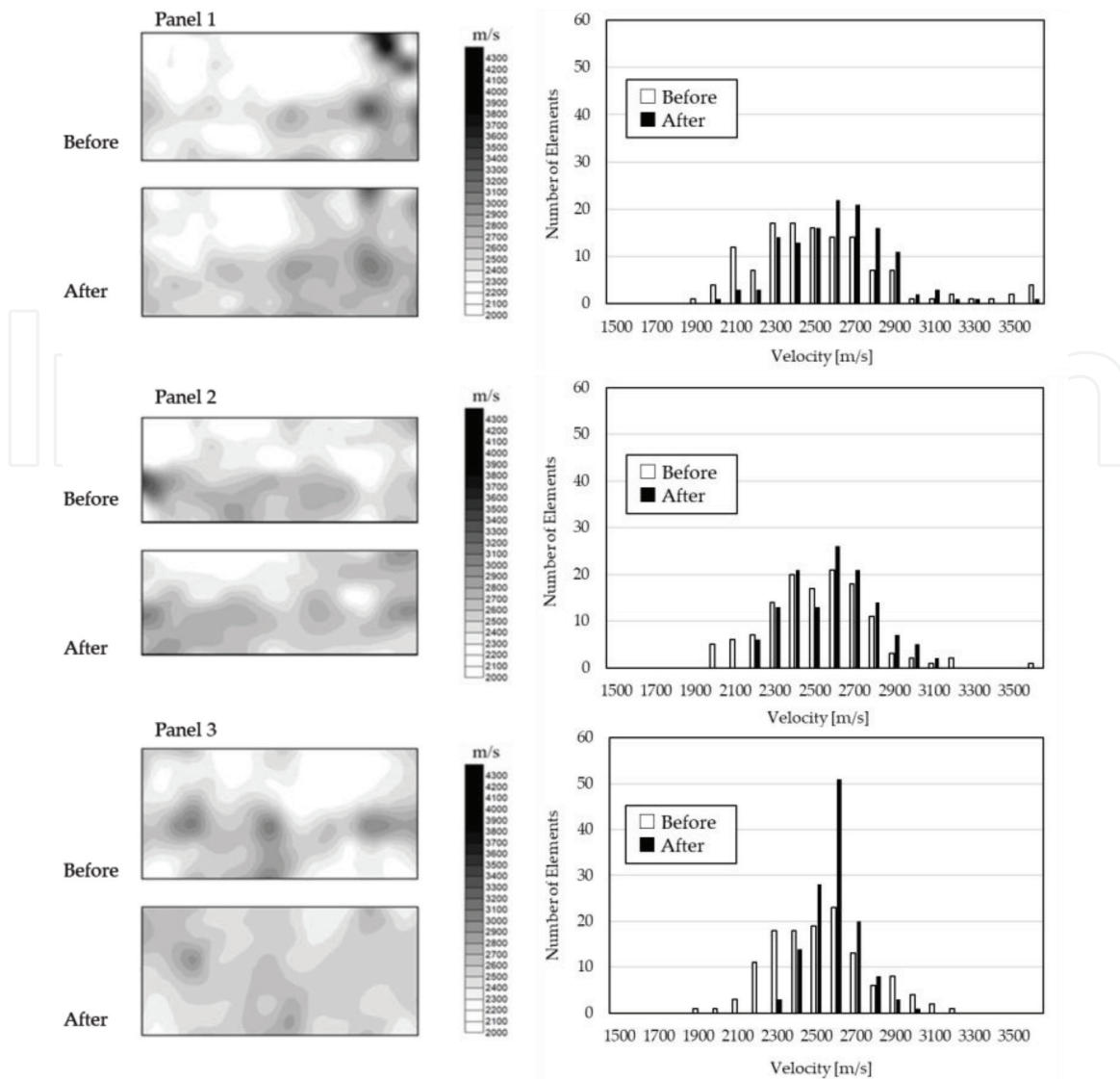


Figure 23.
Results of velocity distribution before and after repair.

repair exhibits increase compared to that before repair. Further quantitatively, the histograms of velocities obtained in all the elements are shown on the right side of the figure. For all slab panels, it is evident that the velocities at the elements clearly shift to the higher regions after repair. Due to the effectiveness of injected material in filling cracks and defects, detours and dispersions in the propagation paths of elastic waves are so eliminated that apparent velocities are increased.

All results imply that the velocity distribution obtained by the AE tomography method has a good potential to be an indicator for ascertaining the filled situation of injected material in a concrete slab. It is confirmed that the velocity for concrete which is not damaged shows about 3500 m/s to 4000 m/s. In some areas, however, velocities of about 2600 m/s are observed even after repair. This is because injected material might not be injected well into continuous cracks, independent air bubbles could be present due to the use of the air-entraining agent, and fine cracks at the interface between coarse aggregate are nucleated due to the alkali-silica reaction. As a result, there exists a possibility that the velocity recovery does not reach to the satisfactory level even after injection. On this issue, we plan to carry out a material test in the laboratory for confirmation.

4.3.2 Relationship between velocity and injection amounts

Design of the injection amount for the crack injection method could be based on the estimation of the crack widths, the depths, and the length measured. It is recognized that there exists no reasonable relationship between the amounts of designed injection and actual injection. Thus, an attempt to examine the amount of injected material is made from the results of AE tomography before repair.

It is considered that the amount of injection should increase, depending on the extent of damage. Namely, if the degree of damage is small, the amount should decrease. In addition, if the damage is less than a certain degree, the injected material may not work well on the damage. On the other hand, if the elastic wave velocity could reflect the degree of damage, a correlation should be evident between

V_P (m/s)	Quality
>4570	Excellent
3660–4570	Fine
3050–3660	Acceptable
2130–3050	Unacceptable
<2130	Poor

Table 2.
 Quality indicator (Whitehurst).

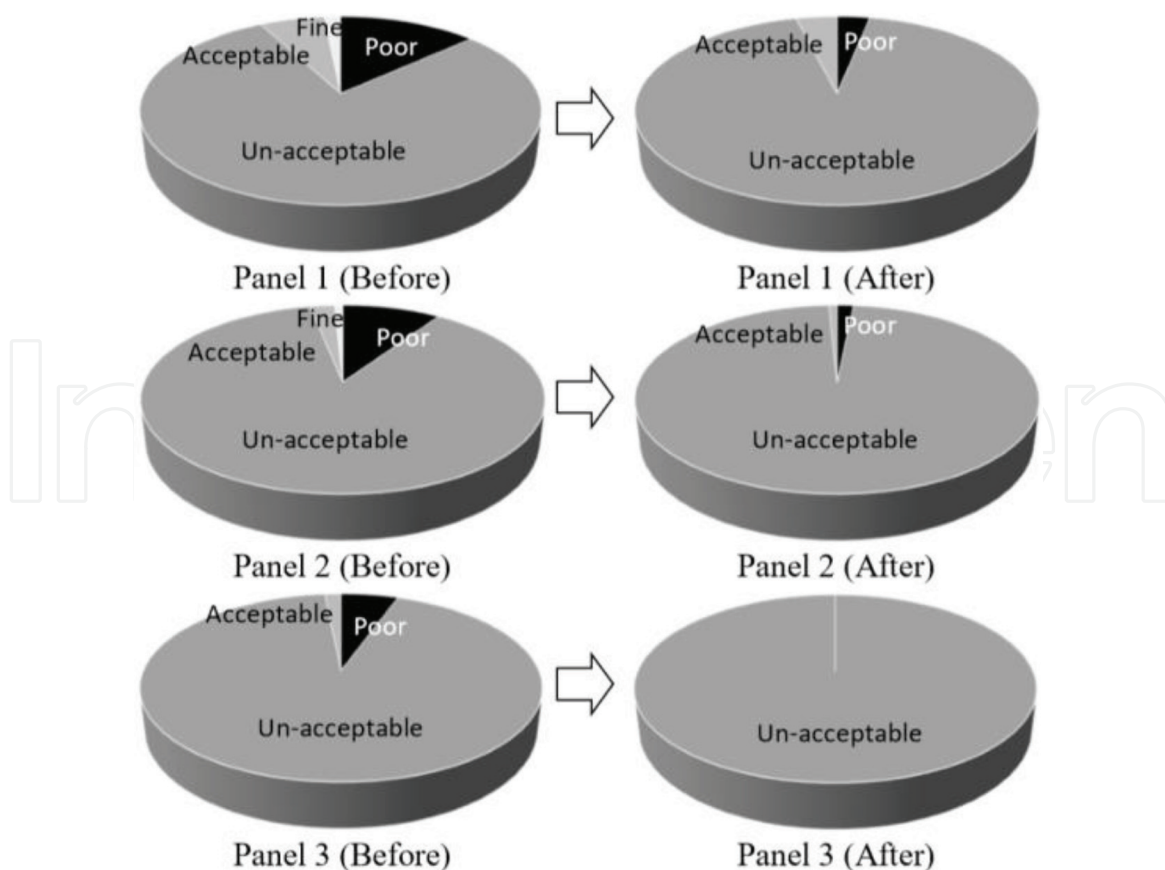


Figure 24.
 Area ratio by quality before and after repair.

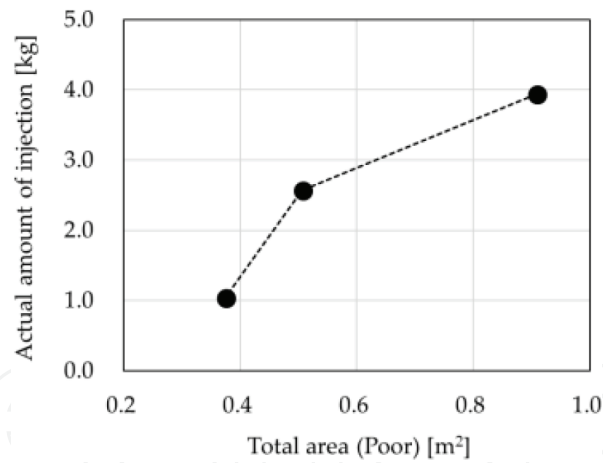


Figure 25.
Total area (Poor) vs. injection amount.

the amount of injection and the values of velocities. Thus, the velocities are classified into grades, as given in **Table 2**. These quality indicators are proposed by Whitehurst [15]. They were determined from the relationship between mechanical properties and P-wave velocity in concrete. Following these indicators, the qualities before and after repair of the panels are classified as shown in **Figure 24**. It is found that the number of elements with Poor decreases, while that of Unacceptable keeps almost the same from before to after repair. As discussed before, due to the presence of air bubbles and the damaged interface with aggregates by alkali-aggregate reaction, the recovery of the velocities may not be apparent. These results imply that the region where the injected material could improve the quality of concrete is mostly that of Poor. It suggests that the repair by means of injection is effective for comparatively major damage. **Figure 25** shows the relationship between total area of Poor estimated by AE tomography before repair and the actual amount of injection. As the Poor area increases, the increase in the actual amount of injection is clearly observed. Thus, it is possible to estimate the amount of injection before repair by carrying out the analysis using AE tomography.

5. Conclusion

Concrete pier, concrete wall, and slab were tested on the investigation on the internal damage assessment for the repair condition by applying elastic wave tomography and AE tomography. Determining the 3D velocity distribution, the repair effects of the epoxy injection method and the patch repair method were quantitatively evaluated. From the results, the following conclusions can be drawn in this study:

1. 3D elastic wave tomography technique can evaluate the penetration of repair epoxy injection material and qualify the repair effect with the amount of injected resin. 3D tomography technique installed with single-side access drill hammering successfully visualizes the internal quality of concrete after the patch repair method based on the elastic wave velocity distribution.
2. The velocity distribution obtained by AE tomography can serve as an indicator for ascertaining the state of crack and void filling with injected material. A good correlation is found between the low velocity region before repair and the

amount of injected material. The results clearly show the potential for the AE tomography technique to be used as a method for estimating the performance of the crack injection method.

As mentioned previously, the RILEM committee was launched because innovative nondestructive inspection testing to qualify repair works is strongly required worldwide. We plan to continue studies based on the evaluation method using elastic wave tomography and accelerate its standardization.

IntechOpen

Author details


Katsufumi Hashimoto^{1*}, Tomoki Shiotani¹, Takahiro Nishida¹
and Nobuhiro Okude^{1,2}

1 Graduate School of Engineering, Kyoto University, Nishikyo-ku, Kyoto, Japan

2 Tokai Technology Center, Higashi-ku, Nagoya, Aichi, Japan

*Address all correspondence to: hashimoto.katsufumi.8a@kyoto-u.ac.jp

IntechOpen

© 2018 The Author(s). Licensee IntechOpen. This chapter is distributed under the terms of the Creative Commons Attribution License (<http://creativecommons.org/licenses/by/3.0>), which permits unrestricted use, distribution, and reproduction in any medium, provided the original work is properly cited. 

References

- [1] Damage assessment in Consideration of Repair/Retrofit-Recovery in Concrete and Masonry Structures by Means of Innovative NDT, Technical Committee IAM, RILEM; http://www.rilem.org/gene/main.php?base=8750&gp_id=347
- [2] Kobayashi Y, Shiotani T, Shiojiri H. Damage identification using seismic travel time tomography on the basis of evolutionary wave velocity distribution model. In: Structural Faults and Repair 2006 (CD-ROM); 2006
- [3] Kobayashi Y, Shiotani T, Aggelis DG, Shiojiri H. Three-dimensional seismic tomography for existing concrete structures. In: Proceedings of Second International Operational Analysis Conference; 2007. Vol. 2. pp. 595-600
- [4] Kobayashi Y, Shiotani T. Seismic tomography with estimation of source location for concrete structure. In: Structural Faults and Repair 2012, CD-ROM; 2012
- [5] Asuae H, Shiotani T, Nishida T, Watabe K, Miyata H. Applicability of AE tomography for accurate damage evaluation in actual RC bridge deck. In: Structural Faults & Repair Conference, No.1743; 2016
- [6] Kobayashi Y, Shiotani T. Computerized AE tomography, innovative AE and NDT techniques for on-site measurement of concrete and masonry structures. In: State-of-the-Art Report of the RILEM Technical Committee 239-MCM; Springer: 2016. pp. 47-68
- [7] Akaike H. Markovian representation of stochastic processes and its application to the analysis of autoregressive moving average processes. *Annals of the Institute of Statistical Mathematics*. 1974;26(1): 363-387
- [8] Zhang H, Thurber C, Rowe C. Automatic P-wave arrival detection and picking with multiscale wavelet analysis for single-component recordings. *Bulletin of the Seismological Society of America*. 2003;93(5):1904-1912
- [9] Osawa S, Shiotani T, Kitora H, Momiyama Y. Damage visualization of imperfectly-grouted sheath in PC structures. In: 31st Conference of the European Working Group on Acoustic Emission, German Society for Non-Destructive; 2014. <http://www.ewgae2014.com/portals/131/bb/fr1b3.pdf>
- [10] Sassa K, Ashida Y, Kozawa T, Yamada M. Improvement in the accuracy of seismic tomography by use of an effective ray-tracing algorithm. In: MMIJ/IMM Joint Symposium Volume Papers; 1989. pp. 129-136
- [11] Kikusui Chemical Industries Co. Ltd. Inside Pressure Hardening. http://www.kikusui-chem.co.jp/pdf/products/catalog/cat_iph_3.pdf
- [12] Sansalone MJ, Streett WB. *Impact-Echo, Nondestructive Evaluation of Concrete and Masonry*. Ithaca, NY: Bullbrier Press; 1997. pp. 29-46
- [13] U.S. Department of the Interior Bureau of Reclamation Technical Service Center. *Best Practices for Preparing Concrete Surfaces Prior to Repairs and Overlays*; 2012
- [14] American Concrete Pavement Association, *Guideline for Partial-Depth Spall Repair, Concrete Paving Technology*; 1998
- [15] Whitehurst EA. Evaluation of concrete properties from sonic tests. In: *ACI Monograph No.2*; ACI; 1966